AIAA JOURNAL
Vol. 32, No. 1, January 1994

Unsteady Panel Method for Flows with Multiple Bodies Moving Along Various Paths

Thomas F. Richason* and Joseph Katz†
San Diego State University, San Diego, California 92182
and
Dale L. Ashby‡
NASA Ames Research Center, Moffett Field, California 94035

A potential flow based three-dimensional panel method was modified to treat time-dependent conditions in which several submerged bodies can move within the fluid along different trajectories. This modification was accomplished by formulating the momentary solution in an inertial frame of reference, attached to the undisturbed stationary fluid. Consequently, the numerical interpretation of the multiple-body, solid-surface boundary condition and the viscous wake rollup was considerably simplified. The unsteady capability of this code was calibrated and validated by comparing computed results with closed-form analytical results available for an airfoil, which was impulsively set into a constant speed forward motion. To demonstrate the multicomponent capability, computations were made for two wings following closely intersecting paths (i.e., simulations aimed at avoiding mid-air collisions) and for a flowfield with relative rotation (i.e., the case of a helicopter rotor rotating relative to the fuselage). Computed results for the cases were compared to experimental data, when such data was available.

Nomenclature

A_k = panel surface area
B_k, C_k = influence coefficients
b = wing span
C_L = lift coefficient
C_l = section lift coefficient
C_M = pitching moment coefficient
C_m = section pitching moment coefficient
C_p = pressure coefficient, defined by Eq. 15
C_{roll} = rolling moment coefficient, moment/$0.5\rho U_\infty^2 A(b/2)$
C_T = thrust coefficient, thrust/$\rho\pi\Omega^2 R^4$
c = wing chord
$\boldsymbol{F}$ = fluid dynamic force
J = advance ratio ($U_\infty/\Omega R$)
N = number of panels
$\boldsymbol{n}$ = vector normal to panel surface
p = pressure
R = rotor radius
r = radial distance
$\boldsymbol{r}$ = vector (x,y,z)
S = surface area element
t = time
U_∞ = freestream velocity
u, v, w = induced velocity components
$\boldsymbol{V}$ = total velocity vector
$\boldsymbol{V}_0$ = translational velocity of origin
v_{ref} = reference velocity used in the Bernoulli equation
x, y, z = body coordinates
α = angle of attack
Γ = circulation
γ = circulation per unit length
θ = rotation about the y axis
μ = doublet strength
ρ = fluid density
σ = source strength
Φ = velocity potential
ϕ = rotation about the x axis
ψ = rotation about the z axis
Ω = rotation rate of body coordinates (or rotor)
ω = frequency, rad/s

Received Nov. 7, 1992; presented as Paper 93-0640 at the AIAA 31st Aerospace Sciences Meeting, Reno, NV, Jan. 11–14, 1993; revision received May 5, 1993; accepted for publication May 12, 1993. Copyright © 1993 by the American Institute of Aeronautics and Astronautics, Inc. All rights reserved.

*Graduate Student, Department of Aerospace Engineering and Engineering Mechanics. Student Member AIAA.

†Professor, Department of Aerospace Engineering and Engineering Mechanics. Associate Fellow AIAA.

‡Aerospace Engineer, Fixed-wing Aerodynamics Branch, MS 247-1. Member AIAA.

Introduction

TIME-DEPENDENT, three-dimensional flowfields are generally difficult to compute using the full Navier-Stokes equations, particularly if relative motion between solid bodies is involved. To obtain engineering solutions for these types of flowfields, simpler mathematical models must be used. One such simpler model for computing three-dimensional flowfields is the panel method. This method is based on the solution of the potential flow equations and can provide detailed information on the pressure and velocity distribution within the incompressible, attached flow regime. A variety of panel methods differing in their numerical approximation to the governing equations are listed in Ref. 1. It is the goal of this study to demonstrate that panel methods can be applied to unsteady flow problems involving the relative motion of solid bodies.

The panel method used in this study is an evolution of one of the simpler formulations[2] presented in the past for computing the potential flow over complex three-dimensional bodies. Time-dependent versions of this earlier formulation were later developed to treat complicated motion of three-dimensional bodies[3] and the rotation of a propeller relative to a stationary wing.[4] This approach led to the development of the panel method of Ames Research Center (PMARC)[5] in which the main emphasis is placed on time-dependent motions of a solid body and computational efficiency, allowing the program to run on small personal computers. The unsteady motion, at this point, was oriented toward maneuvering airplanes for which the path of the motion is known (prescribed) and the geometry of the body was fixed (with time). However, numerous time-dependent fluid dynamic problems require that various components of the body be subject to different or entirely independent motion, as in the case of propellers and rotors[6–8] or for a wing with an oscillating flap. This unsteady, multibody capabil-

ity greatly increases the complexity of the fluid dynamics problem (and of the potential flow model), requiring dramatic restructuring of the original steady-state panel methods.[2,5]

In the present study the panel method of Ref. 5 was modified to accommodate flows in which various body components may move relative to each other and follow different paths. This required the reformulation of the problem in a stationary frame of reference, which is attached to the undisturbed fluid, rather than following the moving-body frame-of-reference approach used in most steady-state panel codes.[2]

To the best of the authors' knowledge, this feature is included for the first time in a widely used panel method[5] which now can be applied to the analysis of both steady and unsteady flowfields, involving multicomponent bodies having independent motions.

Brief Description of the Fluid Dynamic Model

The following brief description of the mathematical formulation of panel methods is aimed only at highlighting the major steps leading to the numerical formulations and indicating the differences between this and some previous[2–5] methods. More details on the mathematical principles of panel methods can be found in text books such as Ref. 1, and details regarding the development of the PMARC code can be found in Ref. 5.

Panel methods, in general, are based on the assumption that for high Reynolds number and attached flow conditions, the viscous effects are confined within thin boundary layers and wakes. The fluid in the region spanning to infinity, as shown in Fig. 1, is assumed to be inviscid, irrotational, and incompressible over the entire flowfield, excluding the region occupied by several moving bodies and their wakes. The continuity equation in terms of the velocity potential Φ, when specified in the inertial frame (X, Y, Z) and attached to the fluid at rest (bounded by S_∞, where the only motion in the fluid is caused by the local motion of the bodies) becomes

$$\nabla^2\Phi = 0 \tag{1}$$

Note that this selection of the coordinate system is equivalent to the "classical small disturbance" choice of coordinate system. The solution to Eq. (1), subject to the appropriate boundary condition, yields the velocity potential in the whole flowfield. Another interesting observation is that Eq. (1) does not include time derivatives. The time dependency is introduced through the boundary conditions. These boundary conditions state that the velocity normal to the boundaries S_{B1}, S_{B2}, ..., and S_∞ (in Fig. 1) is zero. However, prior to formulating these conditions the kinematics of the problem must be considered.

The global coordinate system (X, Y, Z) shown in Fig. 1 is used for solving the fluid dynamic problem. In addition, each of the moving solid bodies has its own body coordinate system $(x, y, z)_i$. Let $\boldsymbol{V}_{0_i}$ be the translation velocity vector, defined in the (X, Y, Z) system. The position vector from the origin of each body system to a point on the body is $\boldsymbol{r}_i(x,y,z)_i$ and Ω_i is the rotation rate of each body's frame of reference,

$$\Omega_i = (\dot{\phi}, \dot{\theta}, \dot{\psi})_i \tag{2}$$

The momentary (Neumann) boundary condition, which requires zero normal velocity at each point on the body, is satisfied by the equation

$$(\nabla\Phi - \boldsymbol{V}_0 - \Omega \times \boldsymbol{r})_i \cdot \boldsymbol{n}_i = 0 \tag{3}$$

in each body's x,y,z coordinates. The direct proof of this kinematic boundary condition is somewhat more elaborate and more details are presented in Ref. 1.

Another form of the boundary condition [Eq. (3)] can be obtained by observing that the incompressible continuity equation (in integral form) states that the change in mass within a closed boundary is zero, or

$$\int_{S_B} \rho \nabla\Phi \cdot \boldsymbol{n}\, dS = 0 \tag{4}$$

If the surface S_B represents a solid surface (e.g., S_{B1} or S_{B2} in Fig. 1), and if no flow crosses these boundaries, then the internal mass is unchanged (or Φ_{in} = const, where the subscript means inside S_B). Since the global coordinate system (X,Y,Z) in Fig. 1 is attached to the stationary fluid, it is possible to select this constant to be zero inside the closed body

$$\Phi_{in} = 0 \tag{5}$$

Equation (5), when applied inside the solid boundaries, can be viewed as an alternative (called the Dirichlet) boundary condition for Eq. (1). The use of Eq. (5) usually yields a numerically more robust algorithm than the equivalent Neumann boundary condition. In most modern codes either condition can be applied to different components of the solid surfaces. Also note at this point that either Eq. (3) or Eq. (4) is necessary for the solution of Eq. (1) but is not sufficient for a unique solution.

Equation (1) can be solved using Green's second identity (for more details see Ref. 1), which states that a general solution to Eq. (1) can be constructed by integrating the contribution of the basic solutions of source σ and doublet μ distributions over the bodies' surface and their wakes

$$\Phi = \frac{1}{4\pi}\int_{\text{body+wake}} \left[\mu \boldsymbol{n} \cdot \nabla\left(\frac{1}{r}\right) - \sigma\left(\frac{1}{r}\right)\right] dS \tag{6}$$

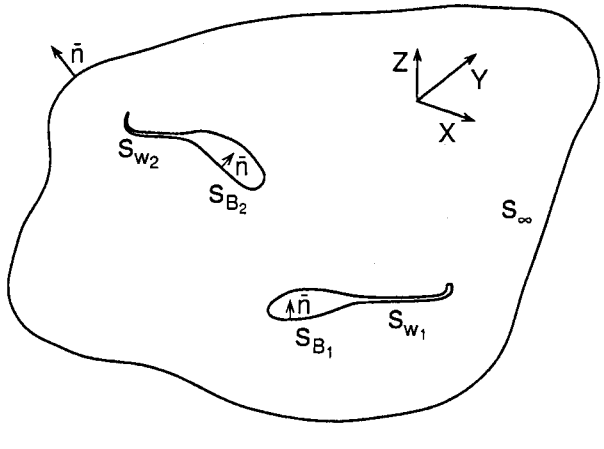

Fig. 1 Nomenclature used to define the potential-flow problem; note that the fluid is stationary in the X, Y, Z coordinates.

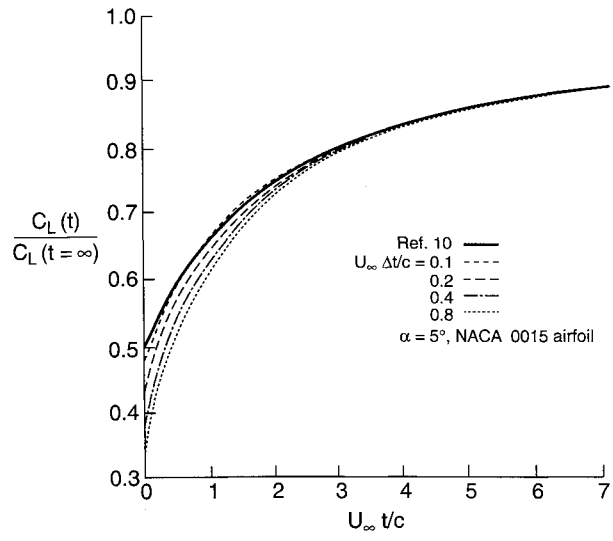

Fig. 2 Effect of time step size on the transient lift coefficient of an infinite-span wing after it was suddenly set into a constant-speed forward motion (airfoil section is NACA 0015).

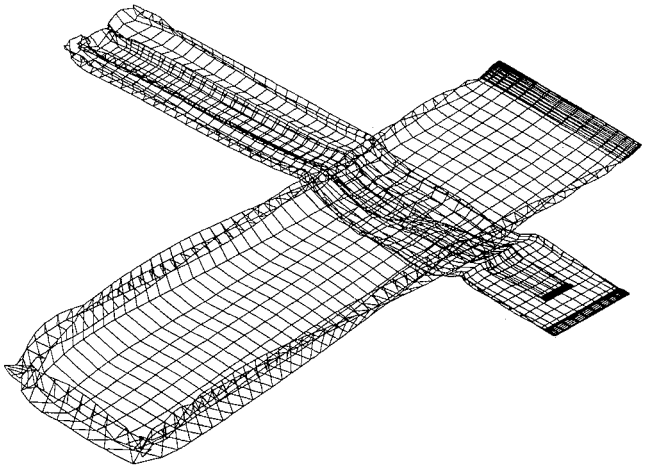

Fig. 3 Two airplanes flying along nearly intersecting paths.

The influence of these singular elements (sources and doublets) decays as the distance r increases from the element (and approaches zero on S_∞ in Fig. 1). Also, note that this solution is provided in the global coordinates (of Fig. 1) whereas the velocity boundary condition [Eq. (3)], at this point, is specified for each body in its own frame of reference.

The modeling of vortex wakes, attached to the lifting surfaces, require some additional conditions. Since potential flow is irrotational, the amount of circulation generated by the various lifting surfaces must be fixed by applying the steady-state Kutta condition along the trailing edges of lifting surfaces

$$\gamma_{TE} = 0 \tag{7}$$

This condition is assumed to be reasonable as long as the flow is attached (and leaves parallel to the trailing edge). The wake shape and rollup can be determined by requiring the vortex wake to be force free, that is, aligned with the local velocity field. If the wake is modeled by closed vortex line elements (which are equal to constant strength, rectilinear doublet elements) then the preceding condition requires that the wake circulation vector γ_W be parallel to the velocity vector V

$$\gamma_W \| V \tag{8}$$

For the unsteady flow case the use of the Kelvin condition will supply an additional equation which can be used to determine the streamwise strength of the vorticity shed into the wake. In general, it states that in the potential flow region, the angular momentum cannot change, thus the circulation Γ around a fluid curve enclosing a lifting surface and its wake is conserved

$$\frac{d\Gamma}{dt} = 0 \tag{9}$$

for any t where Eqs. (8) and (9) are stated in the inertial frame of reference. Again, if the wake is modeled by constant strength doublet panels (closed and fixed-strength vortex lines), then Eq. (9) is implicitly satisfied and does not require additional attention.

A compact solution to Eq. (1) can now be obtained in the global coordinate system by substituting the results of Eq. (6) into the Dirichlet condition [Eq. (5)]. Therefore, inside a closed body

$$\frac{1}{4\pi}\int_{\text{body+wake}} \mu \frac{\partial}{\partial n}\left(\frac{1}{r}\right) dS - \frac{1}{4\pi}\int_{\text{body}} \sigma\left(\frac{1}{r}\right) dS = 0 \tag{10}$$

This equation still does not uniquely describe a solution since a large number of source and doublet distributions will satisfy Eq. (10). To set the strength of the source surface distribution recall that the source represents a discontinuity in the velocity field, thus,

$$-\sigma = \frac{\partial \Phi}{\partial n} - \frac{\partial \Phi_{in}}{\partial n} = \frac{\partial \Phi}{\partial n} \tag{11}$$

since $\partial\Phi_{in}/\partial n = 0$, according to Eq. (5), and Φ is the potential of interest outside the body. Now, substituting $\partial\Phi/\partial n$ from Eq. (3) (where it appears as $\nabla\Phi \cdot \boldsymbol{n}$) into Eq. (11) yields

$$\sigma = -(\boldsymbol{V}_0 + \Omega \times \boldsymbol{r})_i \cdot \boldsymbol{n}_i + V_{\text{norm}} \tag{12}$$

Here the additional velocity V_{norm} is assumed to be known and can be used for modeling jets and boundary-layer thickness effects (by transpiration). At this point, the strength of the source distribution is given by Eq. (12), and the mathematical problem is now unique and can be solved.

To numerically solve Eq. (10), the body's surface S_B is discretized into a set of quadrilateral panels, and constant-strength singularity distributions (of sources and doublets) are assumed on each panel. This formulation, used for the present code (PMARC), is termed a low-order panel method. A high-order panel method would employ a high-order polynomial approximation of either (or both) the singularities or surface shapes. For each of the N surface panels, Eq. (10) [which is another form of the boundary condition of Eq. (5)] is satisfied at a collocation point placed at the center of the panel. Then, for each panel the discretized form of Eq. (10) will be as follows:

$$\sum_{k=1}^{N} C_k \mu_k + \sum_{\ell=1}^{N_W} C_\ell \mu_\ell + \sum_{k=1}^{N} B_k \sigma_k = 0 \tag{13}$$

which must hold at any time t. The coefficients C_k, C_ℓ, B_k in this equation represent the influence of a unit singularity distribution on a panel acting at the collocation point of another panel. If the solid-surface geometry is unchanging with time, C_k and B_k remain constant, although C_ℓ may change if the wake geometry is varied (due to wake rollup). In the present case a relative motion between the various bodies (or surface components) is possible and the coefficients representing the influence of one body on another must be updated at any moment t. Note here that the momentary source strength σ, at each point, can be calculated directly from Eq. (12) and the only time-dependent unknowns are the surface and wake doublet strengths μ_k and μ_ℓ, respectively. However, μ_ℓ is directly related to the surface doublet values of the trailing-edge panels by the Kutta condition. Since Eq. (7) requires that the vor-

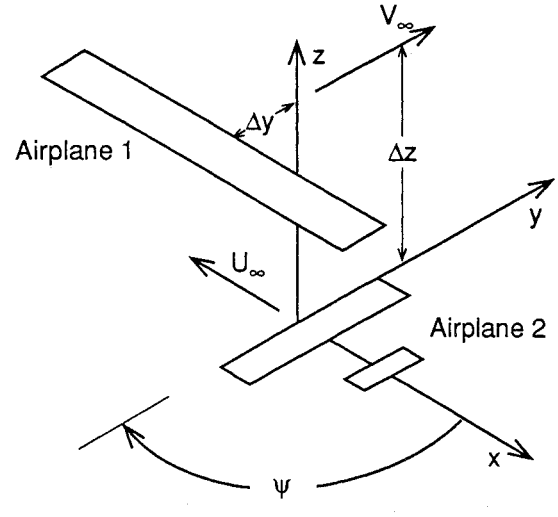

Fig. 4 Details on the geometry used to model the flyby of the two airplanes; note that at $t = 0$, airplane 2 is at the origin and airplane 1 is at $\Delta y/c_1 = 1.36$).

tex strength at the trailing edge must be zero, the strength of the latest wake panel must cancel the two line vortices along the upper and lower trailing-edge panels, or $\mu_\ell = \mu_{upper} - \mu_{lower}$, the relation that reduces the number of unknown doublets to N. Consequently, for N surface panels, Eq. (13) is specified for each of the N collocation points with N unknown doublet values at each moment t, resulting in an algebraic, linear equation of order N.

The application of Eq. (7), as described in the previous paragraph, is in the spirit of the two-dimensional, steady-state Kutta condition, and assumes no pressure jump at a wing's trailing edge. However, the time-dependent, numerical implementation of Eqs. (7) and (8) require additional modeling decisions, such as the angle at which the wake leaves behind a trailing edge and the length of the latest wake panel, with respect to the distance traveled by the trailing edge. These additional parameters were addressed in the past (e.g., in Ref. 9), but in this case the simplest assumption that the latest wake element leaves along the bisector between the trailing-edge upper and lower surfaces was adapted. The length of the latest wake panel was set to one-quarter of the distance traveled by the trailing edge, based on the arguments presented in Ref. 1. These additional conditions are applicable to the latest wake panel only, and the wake rollup procedure described in the next paragraph should, in principle, direct the rest of the wake panels parallel to the local velocity [as in Eq. (8)]. Thus, the effect of fixing the latest wake element direction, relative to the trailing edge, should become negligible when sufficiently small time steps are used (therefore, the maximum time step depends on the streamlines curvature near the trailing edge and can be found by several test runs for each particular case).

The time-dependent numerical solution generally starts as an initial value problem and proceeds as follows. First, the bodies are moved along the prescribed paths (by one time step) and the geometry of the problem is fixed for a given moment [this will automatically set the local source strengths, from Eq. (12)]. Next, the trailing-edge panels where the wakes will be attached are identified as a programmer input. The constant strength doublet panel (which is also used for the wake) is equivalent to a closed vortex ring along the panel edges; therefore, the Kelvin condition [Eq. (9)] is satisfied for all time steps. One wake row is then shed from the specified trailing edges for the first time step. At this point the numerical equivalent of Eq. (13) is in the form of N linear algebraic equations and when solved results in N unknown doublet values (for each of the surface panels). During the next time step, the body's geometry and position are changed according to a prescribed motion and the wake shape is updated (due to wake rollup). To determine the wake rollup at each time step, the induced

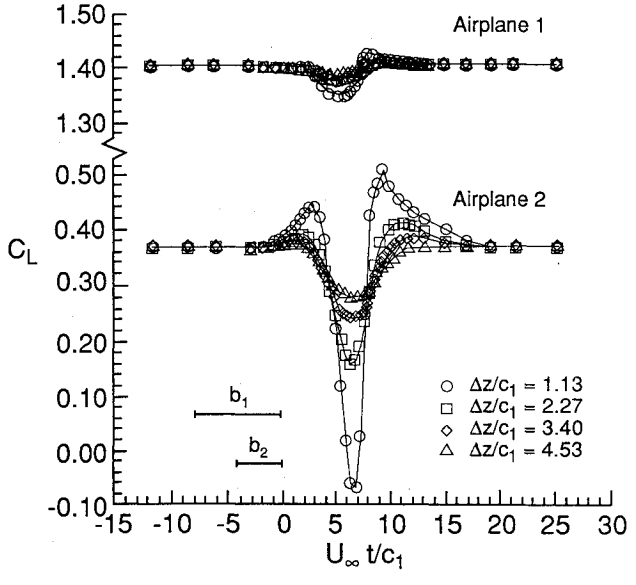

Fig. 5 Lift coefficient variation during the flyby, for several vertical separations.

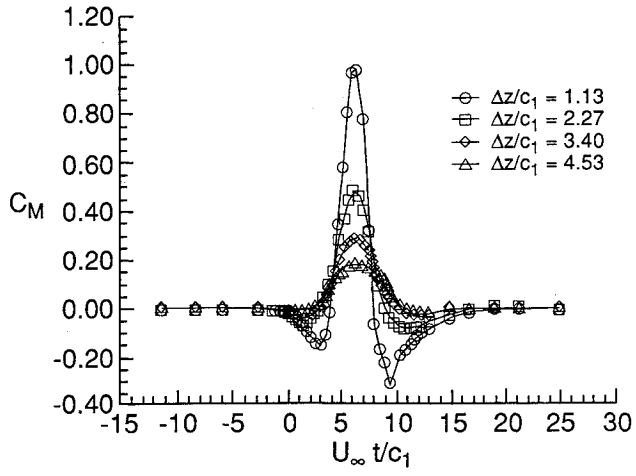

Fig. 6 Pitching moment coefficient variation during the flyby, for several vertical separations.

velocity $(u,v,w)_\ell$ at each wake panel corner point ℓ is calculated (in the undisturbed flow frame of reference). Then, based on an explicit Euler method the vortex elements are moved by

$$(\Delta x, \Delta y, \Delta z)_\ell = (u,v,w)_\ell \Delta t \tag{14}$$

Since both body and vortex wake is modeled by singular source and doublet elements, a vortex core model is used for the wake rollup procedure, which assumes zero velocity when two wake vortices come closer than this core size (which was set equal to $0.001c_1$ in the present case).

The solution of Eq. (13) provides the singularity strengths, which when substituted back into Eq. (6) yields the velocity potential, whereas the gradients of Eq. (6) give the velocity components in the whole fluid region. Once the flowfield velocities are determined, the resulting pressures can be computed using the Bernoulli equation.

$$C_p = \frac{p - p_{ref}}{1/2\,\rho v_{ref}^2} = 1 - \frac{V^2}{v_{ref}^2} - \frac{2}{v_{ref}^2}\frac{\partial \Phi}{\partial t} \tag{15}$$

Here V and p are the local fluid velocity and pressure, respectively; p_{ref} is the far-field reference pressure; and v_{ref} can be selected as the the kinematic velocity [from Eq. (3)]

$$v_{ref} = -[V_0 + \Omega \times r] \tag{16}$$

Note that in situations such as the forward flight of a helicopter, v_{ref} can be selected as the forward flight speed (V_0) or the local speed at each section on the rotor blade. The contribution of a panel with an area of ΔA_k to the aerodynamic loads ΔF_k is thus

$$\Delta F_k = -C_{p_k}(1/2\rho v_{ref}^2)_k \Delta A_k n_k \tag{17}$$

This panel model differs from the methods of Refs. 2–5 by assembling the solution in the stationary fluid frame of reference and allowing multibody, time-dependent motion. This modified formulation has been incorporated into the latest version of the PMARC[5] program.

Sample Results

The simple examples presented in this section served mainly for the validation of the method and helped to demonstrate the capabilities of this approach. The selection of these examples is based on the assumption that the effects of flow separation in the resulting flowfields was negligible. Furthermore, the issue of wake/body or wake/wake impingement was not addressed. The number of

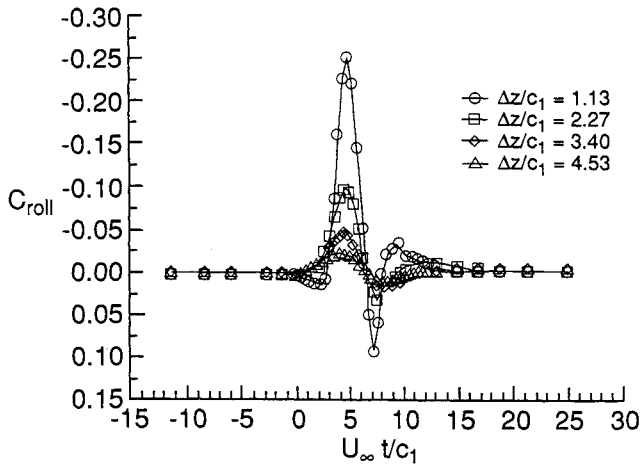

Fig. 7 Rolling moment coefficient variation during the flyby, for several vertical separations.

panels used in these examples represent the minimum number required to capture the flow behavior, based on sensitivity studies carried out in the initial development of the test cases. A sensitivity study determines the minimum number of panels by first generating a solution based on a very sparse paneling of the geometry. The panel density is then increased until the solution does not vary appreciably with an increase in panel density. This final geometry would be the minimum number of panels required for a satisfactory solution in the least computational time. However, based on the limited experience gained during this validation process, it was observed that even for cases requiring more detailed geometry, computational times were still considerably less when compared to other computational methods (e.g., finite difference Navier-Stokes, etc.). Of course, viscous flow information such as the surface skin friction cannot be obtained with this model.

Since panel methods for steady-state flows have been used extensively for a variety of fluid dynamic problems, it is believed that sufficient information exists on the sensitivity of the method to panel density (e.g., Refs. 1–8). However, information in the open literature about the sensitivity of these methods to time step size is far more limited; therefore, the unsteady nature of the code is first validated by comparing the calculated results with the exact solution of Wagner[10] for an impulsively started airfoil (see Fig. 2). In this case a thin, symmetric airfoil is suddenly set into a constant-speed, forward motion, and due to the influence of the starting vortex, the transient lift $C_L(t)$ is less than the steady-state lift, $C_L(t = \infty)$. The solid, thick curve in the figure depicts the exact solution of Ref. 10, clearly displaying that, as the nondimensional time step is being reduced, the numerical solution approaches the exact one. For the numerical computation an NACA 0015 airfoil section was used, and to simulate two-dimensional results a large aspect ratio was selected (AR = 50). The whole wing was modeled by 30 chordwise and 100 spanwise panels totaling 3000 panels. The large difference between the two methods near the origin is due to the infinite acceleration at $t = 0$, assumed in the exact solution. However, in the computations the acceleration takes place within the first time step and, therefore, it is finite and depends on the time step size. Furthermore, during this initial acceleration the lift is much larger and approaches infinity as $\Delta t \to 0$. Because of this large difference in scale (during the first time step), compared with the rest of the data in the figure, the lift during this portion of the acceleration was not plotted on Fig. 2. Based on this figure, time steps on the order of $U_\infty \Delta t/c_1 \approx 0.2$ are sufficient for the cases presented in this paper, and even larger time steps can reasonably capture the transient loads. Additional information on the fluid dynamic aspects of wing's accelerating suddenly into a constant-speed forward motion can be found in Ref. 1.

One possible application of this code's multibody capability is to investigate the interaction between two airplanes flying along different (almost intersecting) paths. In the particular case presented in Fig. 3 the effect of a large airplane's wing on a lighter airplane's stability is investigated. For simplicity, the airplane geometries were represented by simple rectangular wings. To better estimate the effect of the flyby on the smaller airplane's pitching moment, a horizontal tail, which was also modeled as a rectangular wing, was added. The larger airplane's wing was modeled by 408 panels and its lift coefficent was set to $C_L \approx 1.40$, representing a landing configuration. The nearly 16-times smaller airplane's wing and tail were modeled by 646 and 420 panels, respectively, and its cruise lift coefficient was set at $C_L \approx 0.38$. The aspect ratios of the large wing, the small wing, and its tail were 7.25, 6.43, and 3.60, respectively; where the chords were c_1, $0.6c_1$, and $0.38c_1$, with c_1 being the large airplane's chord. Both airplanes had the same forward flight speed, and geometric details of the flyby are presented in Fig. 4. It is clear from this figure that numerous other parameters such as the path intersection angle (shown as Ψ on Fig. 4), the timing of the arrival of each wing to the intersection point, and the various separation distances (Δx, Δy, Δz) are important. For the purpose of demonstrating the capability of the method, only the parameter Δz shown in Fig. 4 will be varied. Finally, the two airplanes in these computations followed a prescribed straight flight path. Therefore, the effect of the aerodynamic interaction on the flight dynamics was not included. However, this capability can be included in future studies.

The effect of the wake/wing induced downwash can be seen in Fig. 3 (Ψ = 90 deg) by observing the downward displacement of the smaller airplane's wake, which passes underneath the wake of the larger airplane ($\Delta z/c_1 = 1.13$). The numerical solution for the present model can be started as an initially steady-state problem or as a sudden acceleration problem. For the latter case, a strong starting vortex should rollup near the initial location of the trailing edge; and the transient influence of this vortex has a considerable and long lasting effect on the solution, as implied by Fig. 2. Therefore, for this case the first option of starting the computations with an initially steady-state solution was used, which also explains the slight discontinuity in the wake rollup pattern near the $t = 0$ point. The magnitude of the interaction in terms of the aerodynamic coefficients vs the nondimensional time $U_\infty t/c_1$ (where c_1 is the larger aircraft wing chord) is presented in the following figures. The geometrical details of this flyby were dictated by an actual mid-air interaction that was simulated by the given model and the $t = 0$ condition is described in Fig. 4. Therefore, at $U_\infty t/c_1 = 0$ the large airplane was at a distance of $\Delta y/c_1 = 1.36$ to the left of the lower airplane's centerline. This case was run for several vertical separa-

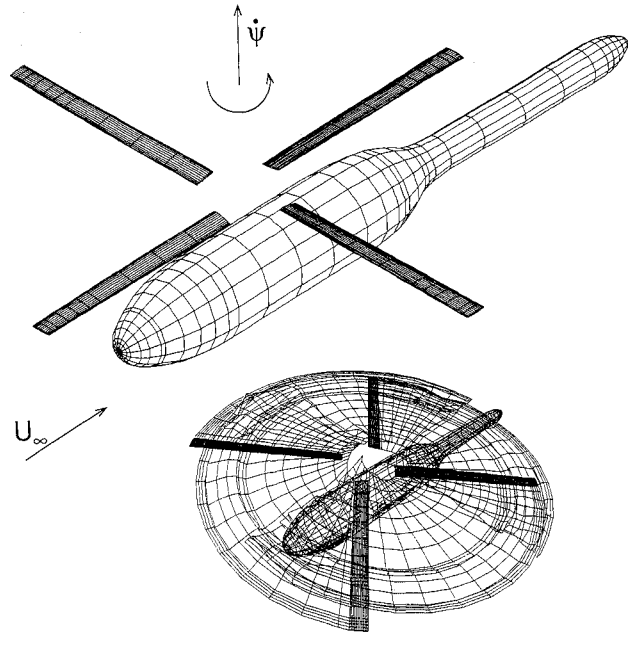

Fig. 8 Panel model of a generic helicopter body and a rotor.

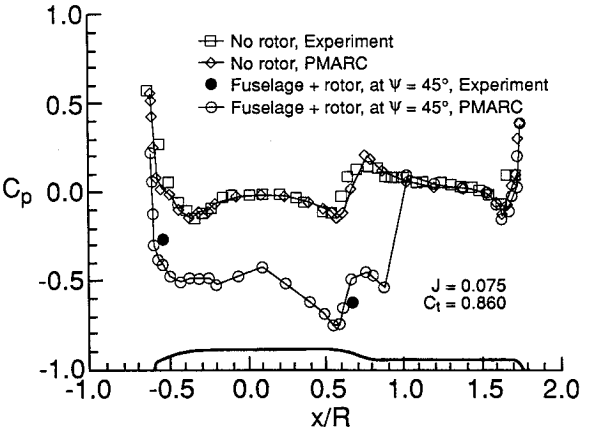

Fig. 9 Pressure distribution along the body's upper centerline without the rotor (diamond and rectangular symbols, steady state) and with the rotor passing through the Ψ = 45 deg position (circles; time dependent, momentary data).

tions of $\Delta z/c_1$. Since both airplanes fly at the same speed ($|U_\infty| = |V_\infty|$), at $t = 1.36c_1/U_\infty$ the large airplane leading edge has reached the lower airplane's centerline, but now this airplane's wing leading edge has moved by $1.36c_1$ forward. The effect of the aerodynamic interaction on the lift of both airplanes is shown in Fig. 5, which indicates that prior to the smaller airplane passing under the larger wing, its lift coefficient increases due to the upwash of the large wing/wake vortex system. But when it flies past the tip, under the upper wing, the downwash prevailing in that area reduces its lift. As the vertical separation Δz decreases, the above described interaction increases, so that at $\Delta z/c_1 = 1.13$, the lift loss (at $U_\infty t/c_1 \approx 7$) is larger than the steady-state lift coefficient of the small airplane. It should be noted that this result may be different if the airplane path was altered by the dynamic effects caused by this large change in C_L.

The effect of the interaction on the larger wing (labeled airplane 1 in the upper part of the figure) is similar in shape but much smaller in magnitude. Therefore, the pitching and rolling moment data will be presented only for the smaller airplane. The pitching moment data (relative to the main wing's quarter chord) of Fig. 6, in principle, follows trends similar to the lift data in Fig. 5. The initial upwash of the wing-tip wake of the larger airplane induces upwash on the smaller airplane's tail, increasing the negative pitching moment (at $U_\infty t/c_1 \approx 3$ the wing has already crossed the imaginary line coinciding with the right wing-tip vortex whereas the tail is still outside this line). As the smaller airplane passes under the wake of the larger wing, its tail is subject to the downwash from the larger wing and its two tip vortices, resulting in a large pitch-up moment. As the tail crosses the shadow of the larger wing's left-hand-side wing-tip wake, it experiences an upwash (at $U_\infty t/c_1 \approx 9$) that gradually decreases as the two wings part.

The rolling moment history during the flyby is presented in Fig. 7. It is seen that as the airplanes approach each other, the upwash induced by the larger airplane is greater on the smaller airplane's left side, resulting in an increasing rolling moment (at $U_\infty t/c_1 < 2$). However, as the smaller airplane slides under the larger airplane, this trend is reversed (before the crossing) and once the small airplane moves behind the upper wing (e.g., at $U_\infty t/c_1 \approx 6$–7) its rolling moment becomes positive again. Then, as the small airplane crosses under the left trailing-edge wake of the larger airplane, the trend reverses and slowly decays to the steady-state condition. If the aileron control limits of the smaller airplane are estimated to be $C_{roll} = \pm 0.03$, then for vertical separations of less than $\Delta z/c_1 \approx 3.5$ the small airplane can lose its stability and control during the flyby. The described variations in the rolling moment are a direct result of the downwash induced by the large wing bound vorticity and the proximity between the two airplanes. Therefore, this effect is not expected to be present in a case when the smaller airplane's path crosses the far-field trailing wake created by the larger airplane. Finally, as expected, for all data presented in regards to this flyby, the effect of interaction clearly becomes smaller as the separation distance increases.

One of the most common flowfields involving relative motion of solid body components is created by rotating propellers[6] and rotors. In these cases, a body usually moves along a straight path, whereas a second component (e.g., a rotor) is rotating relative to an axis fixed to the body. As an example, a panel model of the rotor/body combination (used for the experiments of Ref. 11) was prepared. This model is shown in Fig. 8, and the rotor wake after about one-third revolution is shown on the inset to this figure. The generic body was modeled by 490 panels and 612 panels were used for each rotor, resulting in a total of 2938 panels for the complete configuration. The body has an axisymmetric shape and the four rotor blades have a linear twist of 13 deg from tip to root, with the larger angle at root (refer to Ref. 11 for further details on the geometry). Several pressure transducers were nested along the fuselage (in the experiments of Ref. 11) and time-dependent pressure fluctuations were recorded. The case which served for the following comparison had a rotor advance ratio of $J = 0.075$. The rotor/body was pitched down by 12 deg, resulting in a measured thrust coefficient of $C_T = 0.86$. Calculated and measured pressure distributions along the upper fuselage centerline for the rotor on and rotor off case are shown in Fig. 9. The flow in the rotor off case is independent of time and the computed and experimental data compare well. With the rotor on, the flow becomes time dependent and the momentary, computed pressure distribution along the fuselage centerline (at a rotor blade position of Ψ = 45 deg) is also presented in Fig. 9 (at the time of this comparison only two experimental data points were available). The effect of the rotor, as shown by the computations, is to increase the velocity in the range $x/R = \pm 1.0$, which in turn reduces the local pressure coefficient. It should be noted that the pressure coefficient in Figs. 9–11 is based on the definition used in Ref. 11, that is, $C_p = 200(p - p_\infty/\rho(\Omega R)^2$.

The transducers that were placed on the body in the experiments of Ref. 11 recorded time-dependent fluctuations which reflect four peaks per rotor revolution (due to the four blades). Such data is presented in Fig. 10 for the first transducer (corresponding to the data of Ref. 11) and the location of this transducer is shown in the inset to this figure. The nature of the fluctuations is captured by the computations but at the beginning of the rotor rotation (first rotation) the pressures were displaced by a constant value (see smaller circles on figure). When adding the effect of the downwash created by a fully developed wake (usually requiring about 6–8 rotor rotations[3]), the magnitude of which was approximated here by a method similar to rotor disk theory (e.g., as used in the code of Ref. 2), the computed and experimental data match well, as shown

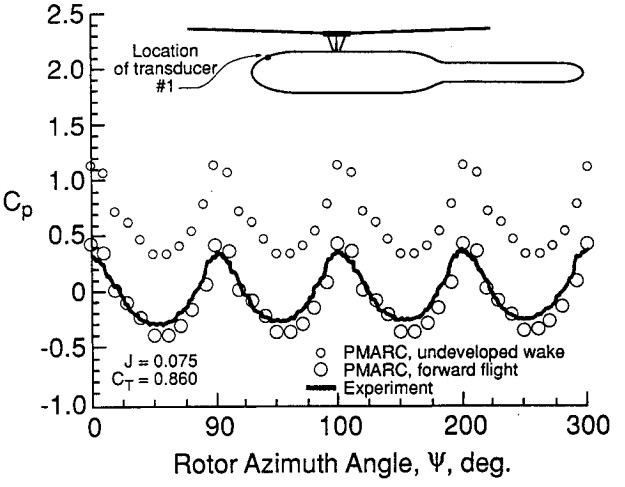

Fig. 10 Comparison between calculated and measured periodic pressure coefficient variation, at transducer location 1, during rotor rotation, in forward flight.

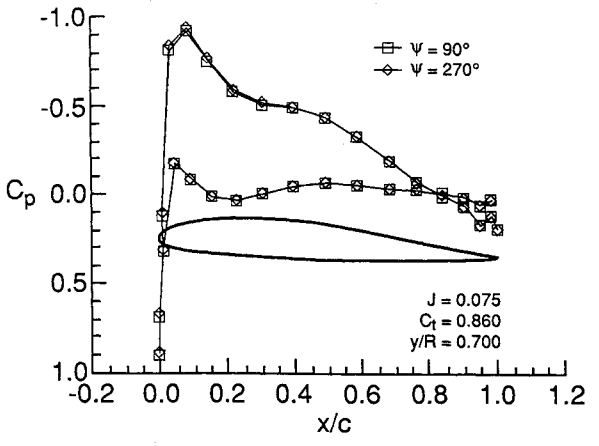

Fig. 11 Calculated pressure distribution for the advancing and retreating blades at a radial station $y/R = \pm 0.7$; airfoil shape is shown by the inset to this figure.

in the lower part of the figure. This downwash approximation was also applied to the results presented in the rotor/body case shown in Fig. 9. In general, at the lower advance ratios the rotor wake contacts the helicopter body, resulting in local flow separations. This effect of wake impingement on the fuselage requires additional modeling and considerably more computational effort (due to more rotor rotations), therefore, was not attempted at this early stage of model validation.

Information on rotor blade section pressure distribution is necessary when developing airfoil sections for rotorcraft application, and such computed data is shown in Fig. 11 (no similar experimental data was available). The difference between the advancing and retreating blade is marginal because of the low forward-flight speed (relative to the blade-tip speed, or small J), and the flow is most likely attached in both cases. Also, the whole geometry was pitched down by 12 deg, which caused a smaller effective angle of incidence on the advancing blade while increasing the effective incidence on the retreating blade. Of course many rotorcraft flight conditions involve regions of separated flows and then the present method is not applicable.

Conclusions

The examples investigated in this study demonstrate the capability of the present method to model fairly complex attached flowfields such as those created by the unsteady motion of wings moving in different directions and by the rotation of rotors relative to a helicopter body. Calculated pressure distributions and loads compare favorably with the limited experimental data that was available for validating this time-dependent method.

The overall approach is limited only by the restrictions of the potential flow model, which is applicable mainly to high-Reynolds number, incompressible, attached flows. However, problems such as wake impingement on solid surfaces, as in the case of a puller or counter-rotating propellers, was not addressed. Future modeling efforts can focus on this area as well as on coupling this aerodynamic model with a vehicle dynamic model for flight-path calculations.

Acknowledgment

This work was supported by NASA Ames Research Center, under Grant NCC-2-676, with Dale L. Ashby as Project Monitor.

References

[1]Katz, J., and Plotkin, A., *Low-Speed Aerodynamics: From Wing Theory to Panel Methods*, McGraw-Hill, New York, 1991, Secs. 3.2, 12.4, 13.1, 13.8.2, and pp. 491–494.

[2]Maskew, B., "Program VSAERO, A Computer Program for Calculating the Nonlinear Aerodynamic Characteristics of Arbitrary Configurations," NASA CR-166476, Nov. 1982.

[3]Katz, J., and Maskew, B., "Unsteady Low-Speed Aerodynamic Model for Complete Aircraft Configurations," *Journal of Aircraft*, Vol. 25, No. 4, 1988, pp. 302–310; also AIAA Paper 86-2180, Aug. 1986.

[4]Rangwalla, A. A., and Wilson, L. N., "Application of a Panel Code to Unsteady Wing-Propeller Interference," *Journal of Aircraft*, Vol. 24, No. 8, 1987, pp. 568-570.

[5]Ashby, L. D., Dudley, M. D., Iguchi, S. K., Browne, L., and Katz, J., "Potential Flow Theory and Operation Guide for the Panel Code PMARC," NASA TM 102851, March 1990.

[6]Yon, S., Katz, J., and Ashby, D., "Unsteady Fluid Dynamic Model for Propeller Induced Flow Fields," AIAA Paper 91-1664, June 1991.

[7]Lee, Y. J., and Yang, J. Y., "A Panel Method for Arbitrary Moving Boundaries Problems," *AIAA Journal*, Vol. 27, No. 3, 1990, pp. 432–438.

[8]Kinnas, S. A., and Hsin, C. Y., "Boundary Element Method for the Analysis of the Unsteady Flow Around Extreme Propeller Geometries," *AIAA Journal*, Vol. 30, No. 3, 1992, pp. 688–696.

[9]Basu, B. C., and Hancock, G. J., "The Unsteady Motion of a Two-Dimensional Aerofoil in Incompressible Inviscid Flow," *Journal of Fluid Mechanics*, Vol. 87, Pt. 1, 1978, pp. 159-178.

[10]Wagner, H., "Uber die Entstehung des Dynamischen Autriebes von Tragflugeln," *Zeitschrift für Angewandte Mathematic und Mechanic*, Vol. 5, No. 1, Feb. 1925, pp. 17–35.

[11]Bi, N., Leishman, J. G., and Crouse, G. L., Jr., "Investigation of Rotor Wake Interactions with a Body in Low Speed Forward Flight," AIAA Paper 91-3228, Sept. 1991.